Supporting Information

Ultrafast-charging Quasi-solid-state Fiber-shaped Zinc-ion Hybrid Supercapacitors with Superior Flexibility

Jie Pu,[a] Qinghe Cao,[a] Yong Gao,[a] Jie Yang,[b] Dongming Cai,[a] Xing Chen,[c] Xiaowan Tang,[a] Gangwen Fu,[a] Zhenghui Pan,[ab]*, and Cao Guan,[a]*

[a]*Frontiers Science Center for Flexible Electronics, Institute of Flexible Electronics, Northwestern Polytechnical University, Xi'an 710072, P. R. China*

[b]*Department of Materials Science and Engineering, National University of Singapore, 9 Engineering Drive 1, Singapore 117576, Singapore*

[c]*Shaanxi Engineering Research Center for Digital Manufacturing Technology, Northwestern Polytechnical University, Xi'an 710072, P. R. China*

** Corresponding authors*
E-mail: msepz@nus.edu.sg; iamcguan@nwpu.edu.cn.

Experimental section

Materials and Reagents: $Co(NO_3)_2 \cdot 6H_2O$ was purchased from Damas. $Fe(NO_3)_2 \cdot 9H_2O$ and Dicyandiamide (DCDA) were obtained from Aladdin Industrial Corporation. Urea was purchased from Hushi. $ZnSO_4 \cdot 7H_2O$ and ethanol were purchased from Huada. NH_4F was bought from REGENT. PVA was purchased from biofount. $Zn(CF_3SO_3)_2$ was obtained from Macklin. All chemicals were used directly without any further treatment, and all aqueous solutions were prepared using deionized (DI) water.

FE simulation: The finite element simulation illustrating the mechanical robust of 3D nanostructured fiber electrode and comparing the FZHSC woven into a textile substrate under two

deformation states were implemented in commercial package COMSOL. For the first case, we took the CNT nanoarrays (length is 137.5 μm) grown on CNT fiber (radius is 62.5 μm, length is 2.2 mm) as the example and compared its stress distribution with the CNT fiber covered with a layer of carbon material (thickness is 5 μm). The elastic properties of the material refer to CNT, whose elastic modulus is 2.25 GPa and Poisson's ratio is 0.269.[1] The boundary condition was set to fix the middle boundary, and two ends were moved down 10 μm along the Z axis to make it bend. For the second case, all models performed the same area and fiber diameter (100*60 mm^2 and 350 μm). We make the ideal assumption and modeling according to actual condition, and perform linear elastic analysis. In the relaxed state, the left boundary was fixed, and a load was applied to the right boundary to deform the structure and perform buckling analysis. In the bending state, the boundary conditions were set to fix the left and right boundaries, and then applied a load on the bottom surface in the Z-axis direction to bend the structure. The simulation used grid and steady state analysis controlled by the solid mechanics physics. However, the models can only establish an ideal system, and cannot fully reflect the real condition.

Materials Characterization: Samples were characterized using transmission electron microscopy (TEM, FEI Talos F200), scanning electron microscopy (SEM, Zeiss, 5.0–20.0 kV) equipped with an EDX detector, Raman spectra (WITec Alpha300R, 532nm), X-ray photoelectron spectroscopy (XPS, Kratos, Axis Supra) and X-Ray Diffraction (XRD, Bruker D8 advance). The mechanical properties of the fibers were characterized by testing 30 mm long samples at room temperature with a loading speed of 2 mm/min. The number of tensile test samples was more than 5. All tests were carried out on a tensile instrument (Shanghai New Fiber Instrument Co., Ltd, XQ-1C, China).

Electrochemical Characterization: Electrochemical performance of fiber electrodes were

characterized by CV and GCD methods in a three-electrode cell with 1 M $ZnSO_4$ aqueous electrolyte using electrochemistry workstation (CHI 760E). A single N-CNT@CNT fiber or CNT fiber (1 cm), a platinum mesh (1× 1 cm^2), and an Ag/AgCl (3 M KCl) electrode acted as the working electrode, counter electrode, and reference electrode, respectively. The CV curves were obtained at different scan rates. All current densities were normalized the area of the working electrode.

The electrochemical performance of the as-fabricated quasi-solid-state FZHSCs were determined from their CVs at different scan rates and GCD curves at different current densities. The cycling performance measurement was carried out on a NEWARE battery testing system. The areal capacitance of single electrode and device (C_A, mF cm^{-2}) were calculated by Equations (1) from their GCD curves,

$$C_A = \frac{I \times \Delta t}{\Delta V \times A} \tag{1}$$

where I is the discharge current (mA), Δt is the discharge time (s), ΔV is the working potential voltage (V), and A is the geometric electrode working areal (cm^{-2}).

The areal energy density (E_A), volumetric energy density (E_V) and specific energy density (E_m) and the corresponding power density (P_A, P_V and P_m) of device were calculated by Equations (2−7):

$$E_A = \frac{1000}{2 \times 3600} \times C_A \times \Delta V^2 \tag{2}$$

$$P_A = \frac{3600 \times E_A}{t} \tag{3}$$

$$E_V = \frac{1000}{2 \times 3600} \times C_V \times \Delta V^2 \tag{4}$$

$$P_V = \frac{3600 \times E_V}{t} \tag{5}$$

$$E_m = \frac{1000}{2 \times 3600} \times C \times \Delta V^2 \tag{6}$$

$$P_m = \frac{3600 \times E_m}{t} \tag{7}$$

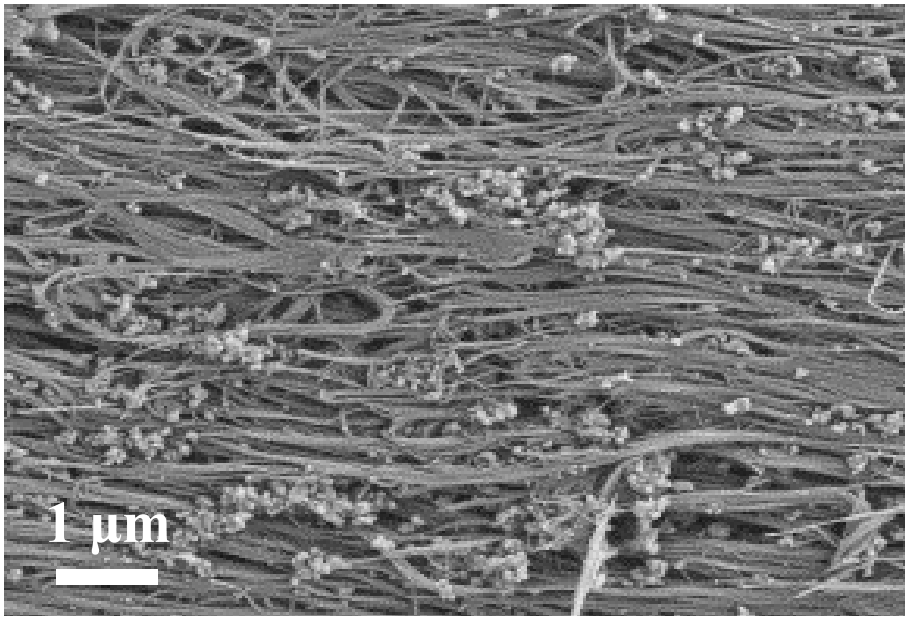

Fig. S1. Magnified SEM image of pristine CNT fiber.

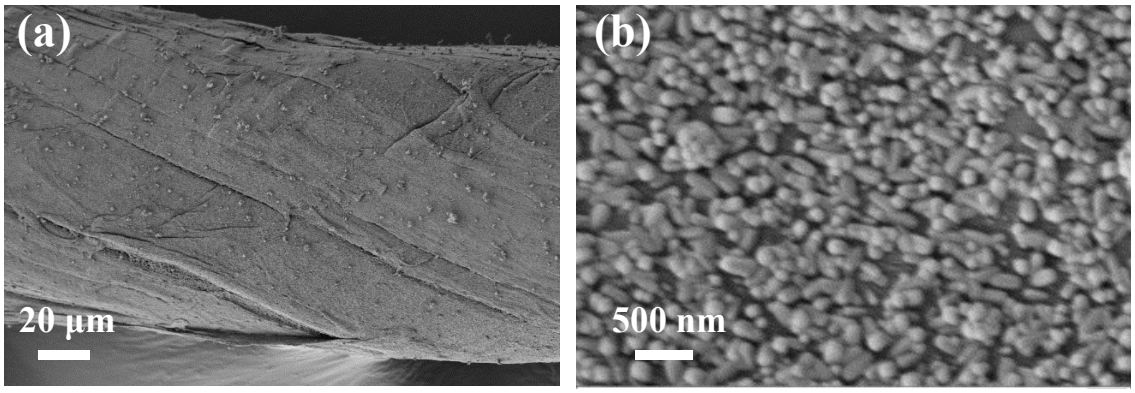

Fig. S2. (a-b) SEM images of CoFe NPs@CNT fiber under different magnifications.

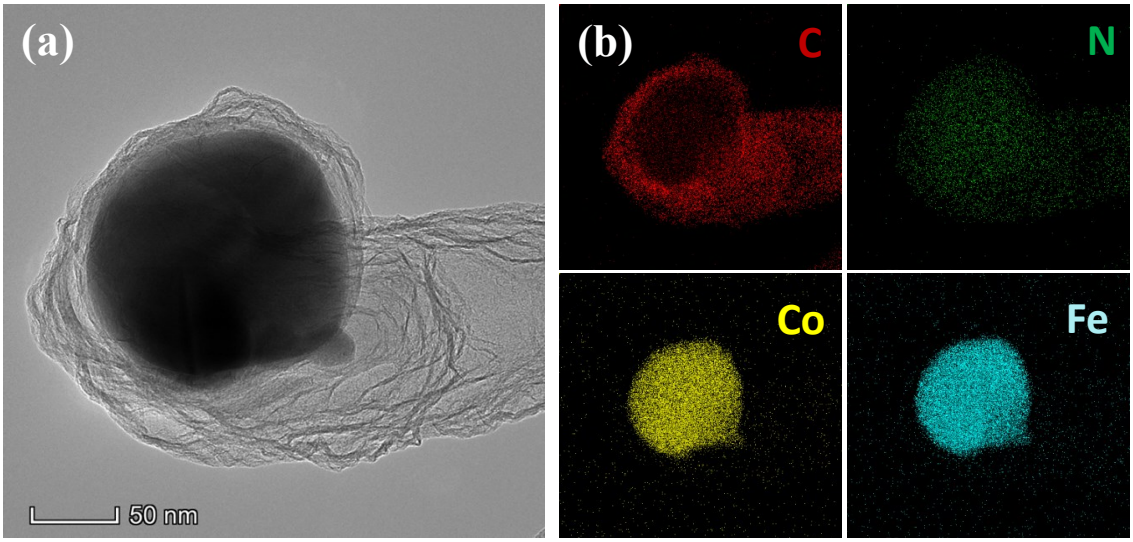

Fig. S3. (a) TEM image of N-CNT. (b) Corresponding elemental mapping images of N-CNT.

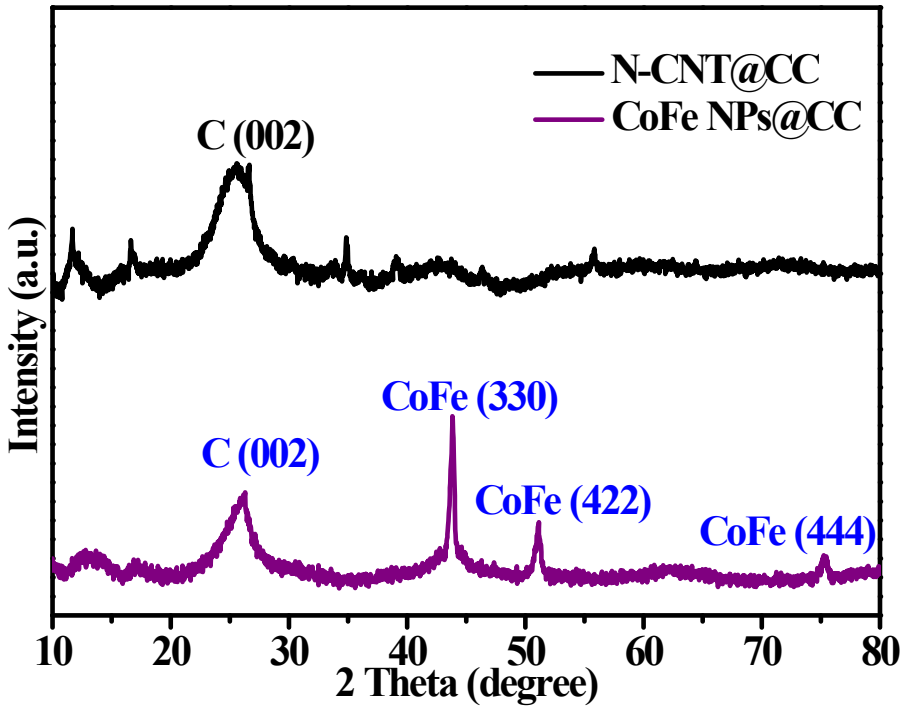

Fig. S4. XRD patterns of CoFe NPs@CC and N-CNT@CC. (Noted: To observe more obvious peak intensity of the bimetallic CoFe, CoFe NPs@CC and N-CNT@CC (carbon cloth) were prepared under the same conditions. CC and CNT fiber only serve as the current collects and will not affect the XRD results of CoFe NPs@CC and CoFe NPs@CNT fiber electrodes.)

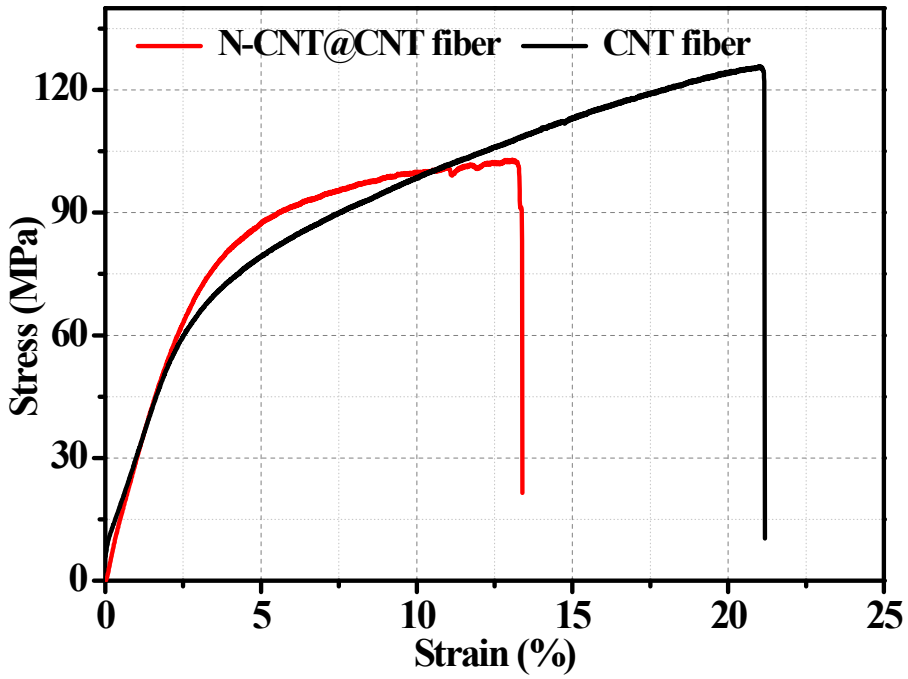

Fig. S5. Comparison of the stress-strain curves of CNT fiber and N-CNT@CNT fiber.

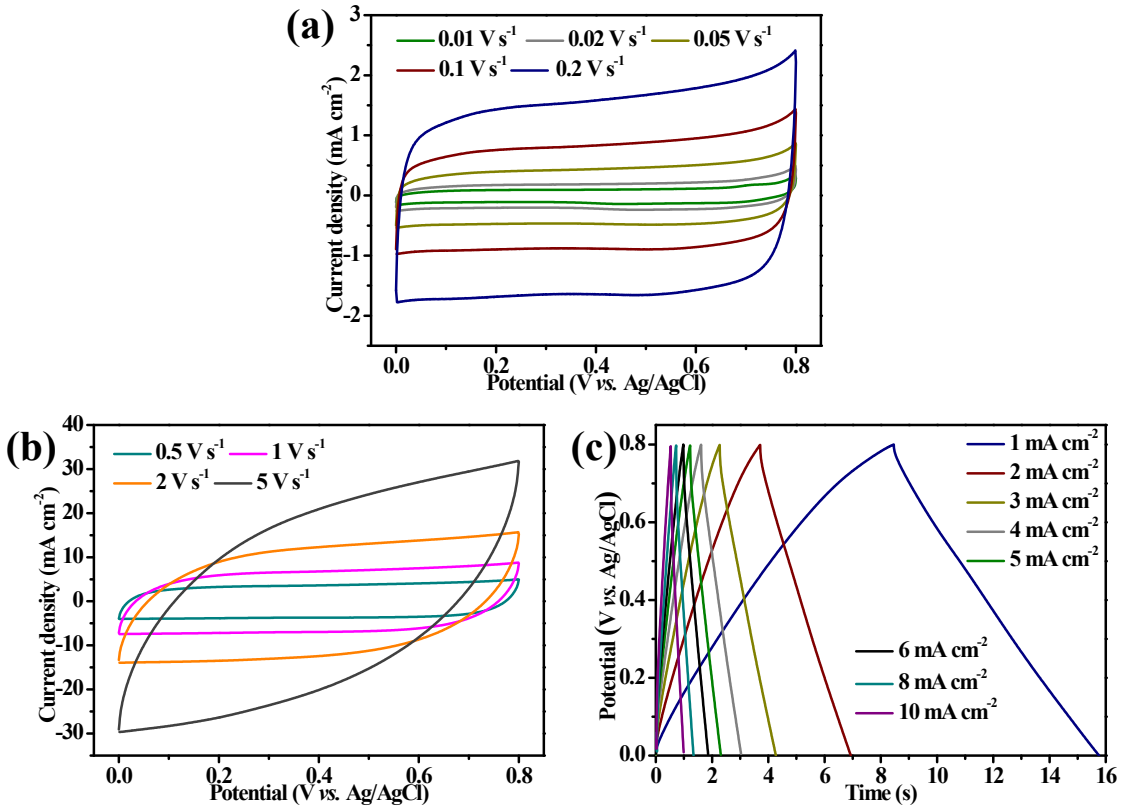

Fig. S6. (a-b) CV curves and (c) GCD curves of the CNT fiber.

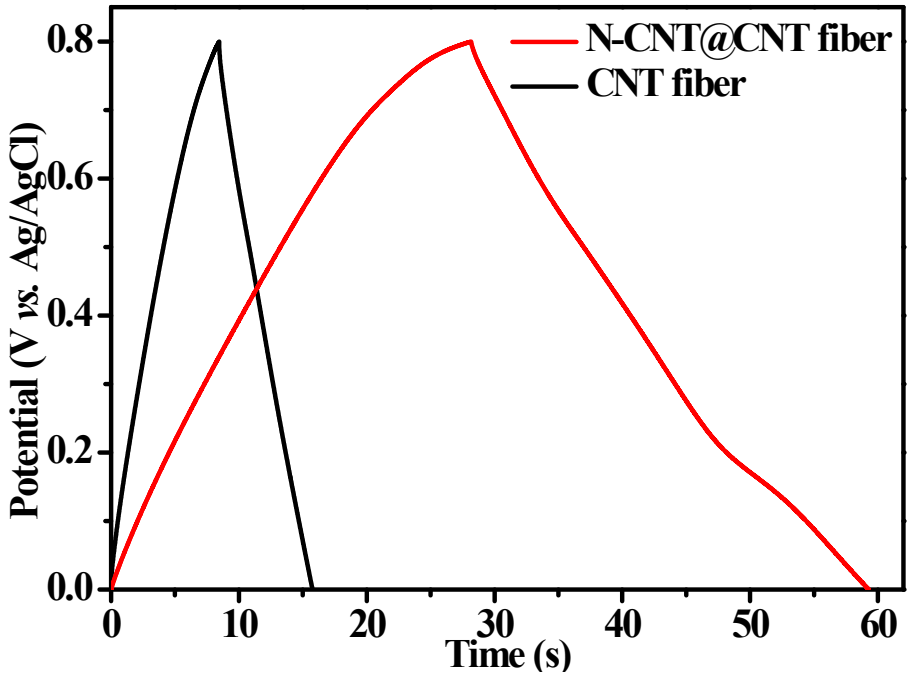

Fig. S7. GCD curves of the two fiber electrodes at 1 mA cm^{-2}.

Table S1. Comparison of the areal capacitance of carbon-based electrodes.

Electrode material	Current density/ Scan rate	Electrode system	Areal capacitance	Ref.
CCNC	1 A g^{-1}	Two	8.8±0.8 μF cm^{-2}	2
ISAC850	0.2 A g^{-1}	Two	13.3 μF cm^{-2}	3
S-carbon	5 mV s^{-1}	Two	10.8 μF cm^{-2}	4
L-carbon	5 mV s^{-1}	Two	14.6 μF cm^{-2}	
CS-carbon	5 mV s^{-1}	Two	12.6 μF cm^{-2}	
CL-carbon	5 mV s^{-1}	Two	39.4 μF cm^{-2}	
AS-carbon	5 mV s^{-1}	Two	14.9 μF cm^{-2}	
AL-carbon	5 mV s^{-1}	Two	14.0 μF cm^{-2}	
NPS-800	5 mV s^{-1}	Two	137.2 μFcm^{-2}	5
GHC-17	0.5 A g^{-1}	Two	15 μF cm^{-2}	6
CK21	0.2 A g^{-1}	Three	25.5 μF cm^{-2}	7
CF-MSP	1 A g^{-1}	Three	13 μF cm^{-2}	8
HPCSLS-700-1	0.05 A g^{-1}	Two	27.4 μF cm^{-2}	9
WB-HPC-700	0.5 A g^{-1}	Three	14.4 μF cm^{-2}	10
NCNT@CNT	**1 mA cm^{-2}**	**Three**	**39 mF cm^{-2}**	**This work**

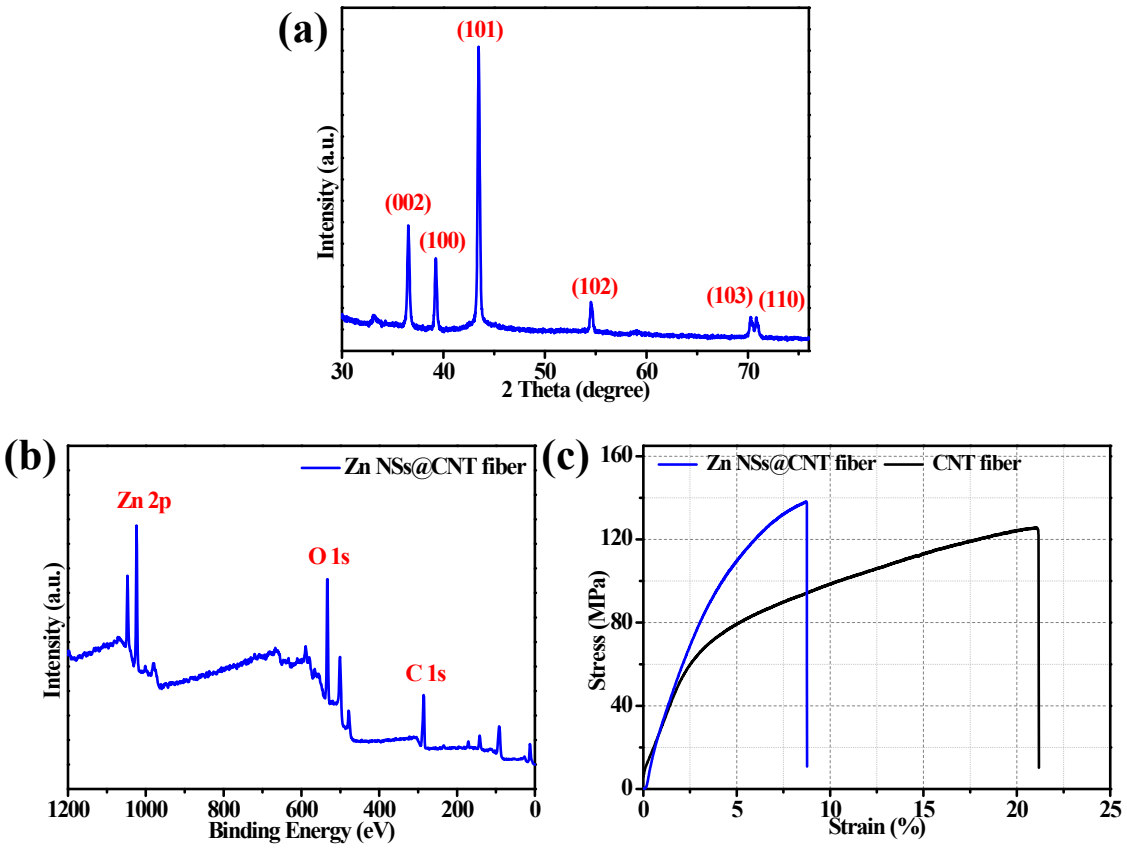

Fig. S8. (a) XRD pattern and (b) XPS spectrum of Zn NSs@CNT fiber. Comparison of the (c) stress-strain curves of the Zn NSs@CNT and CNT fiber.

The electrodeposited Zn NSs with a high crystallinity on CNT fiber can be well in accordance with the hexagonal Zn (JCPDS No. 87−0713) (Figure S8a). The XPS spectrum of Zn NSs@CNT fiber further confirms the successful of obtaining metallic Zn (Figure S8b). In addition, the Zn NSs@CNT fiber possesses a superior tensile strength of 138 MPa (Figure S8c), which can ensure its structural integrity during bending condition.

Table S2. Comparison of the charge/discharge rate of Quasi-Solid-State ZHSCs based on carbon materials.

Device configuration	Electrode material	Scan rate (V s^{-1})	Ref.
Carbon coated aluminum foil	Bio-carbon derived porous material	1 V s^{-1}	11
Micro-supercapacitors	Activated carbon	0.005 V s^{-1}	12
Fiber	rGO/CNT	0.1 V s^{-1}	13
Fiber	Diamond	0.2 V s^{-1}	14
Carbon cloth	rGO	0.02 V s^{-1}	15
Micro-supercapacitors	Kelp carbon	0.1 V s^{-1}	16
Carbon paper	N-doped porous carbon	0.08 V s^{-1}	17
Carbon cloth	Co-polymer derived hollow carbon spheres	0.05 V s^{-1}	18
Graphite paper	B/N co-doped carbon	0.05 V s^{-1}	19
Fiber	**N-CNT@CNT**	**5 V s^{-1}**	**This work**

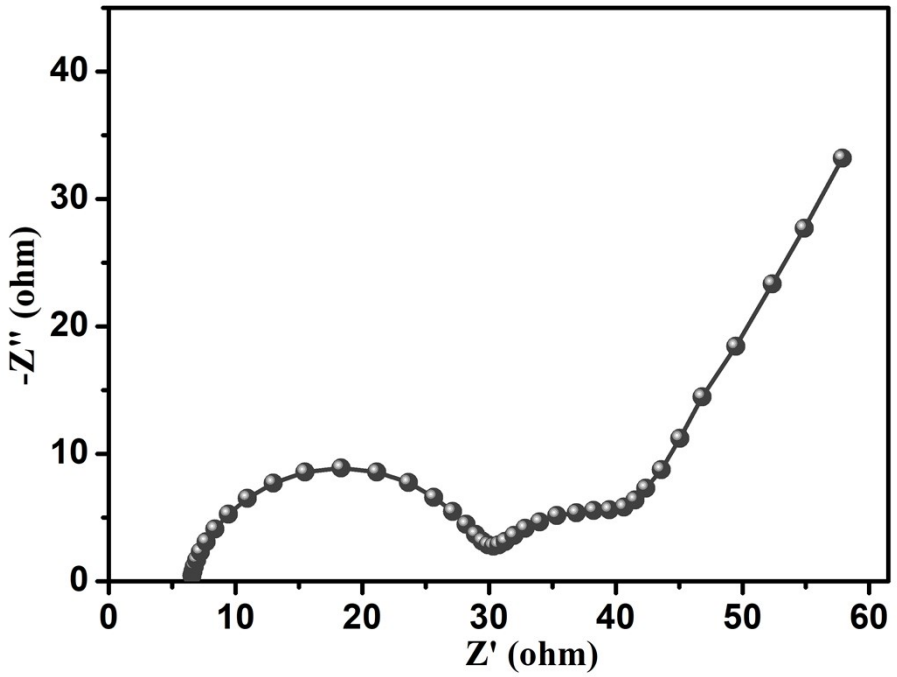

Fig. S9. EIS Nyquist plot for the FZHSC device.

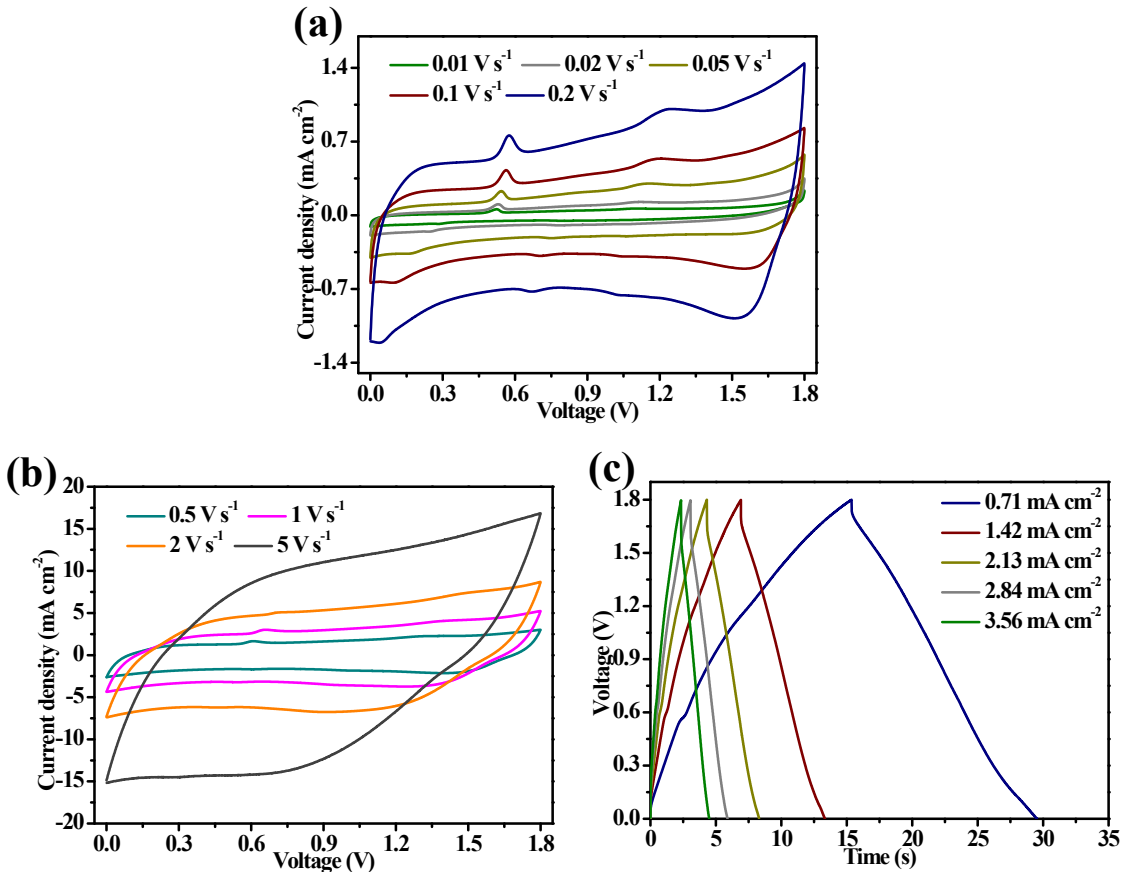

Fig. S10. (a-b) CV curves of the assembled FZHSC with CNT fiber positive electrode measured at different scan rates. (c) GCD curves at different current densities.

Table S3. Summary of voltage window, areal and volumetric energy density (power density) of current study with other reported fiber-based energy storage devices.

Device types (configurations)	Energy storage system (Cathode//Electrolyte//Anode) Operating voltage (V)	$E_{A\text{-}max}$ (μWh cm^{-2})/ $P_{A\text{-}max}$ (mW cm^{-2})	$E_{V\text{-}max}$ (mWh cm^{-3})/ $P_{V\text{-}max}$ (W cm^{-3})	Ref.
Electrical double layer capacitors (Twisted)	3DG@graphene fiber// PVA/H_2SO_4// 3DG@graphene fiber 0–0.8	0.17/0.1	N/A	20
Electrical double layer capacitors (Twisted)	Pen ink@plastic fiber//PVA/H_2SO_4// Pen ink@plastic fiber 0–0.8	2.7/9.07	N/A	21
Electrical double layer capacitors (Twisted)	OMC@CNT fiber//PVA/H_3PO_4// OMC@CNT fiber 0–1.0	1.77/--	N/A	22
Symmetric pseudocapacitors (Twisted)	PEDOT:PSS fiber//PVA/H_3PO_4// PEDOT:PSS fiber 0–1.0	4.13/0.25	N/A	23
Symmetric pseudocapacitors (Coaxial)	MnO_2@AuPd@CuO wire// PVA/KOH // MnO_2@AuPd@CuO wire 0–0.8	N/A	0.55/--	24
Zn–alkaline batteries (Twisted)	NiO@Ni wire//PVA/KOH //Zn wire 1.3–1.9	N/A	0.67/--	25
Commercial 2.75 V/44 mF EDLC	N/A	N/A	0.8/--	26
Commercial 3.5 V/25 mF EDLC	N/A	N/A	0.2/--	26
Fiber-shaped Zinc-ion Hybrid Supercapacitors (Twisted)	**NCNT@CNT //Zn$(CF_3SO_3)_2$/PVA//Zn NSs@CNT fiber 1.8 V**	**5.18/3.22**	**0.92/0.58**	**This work**

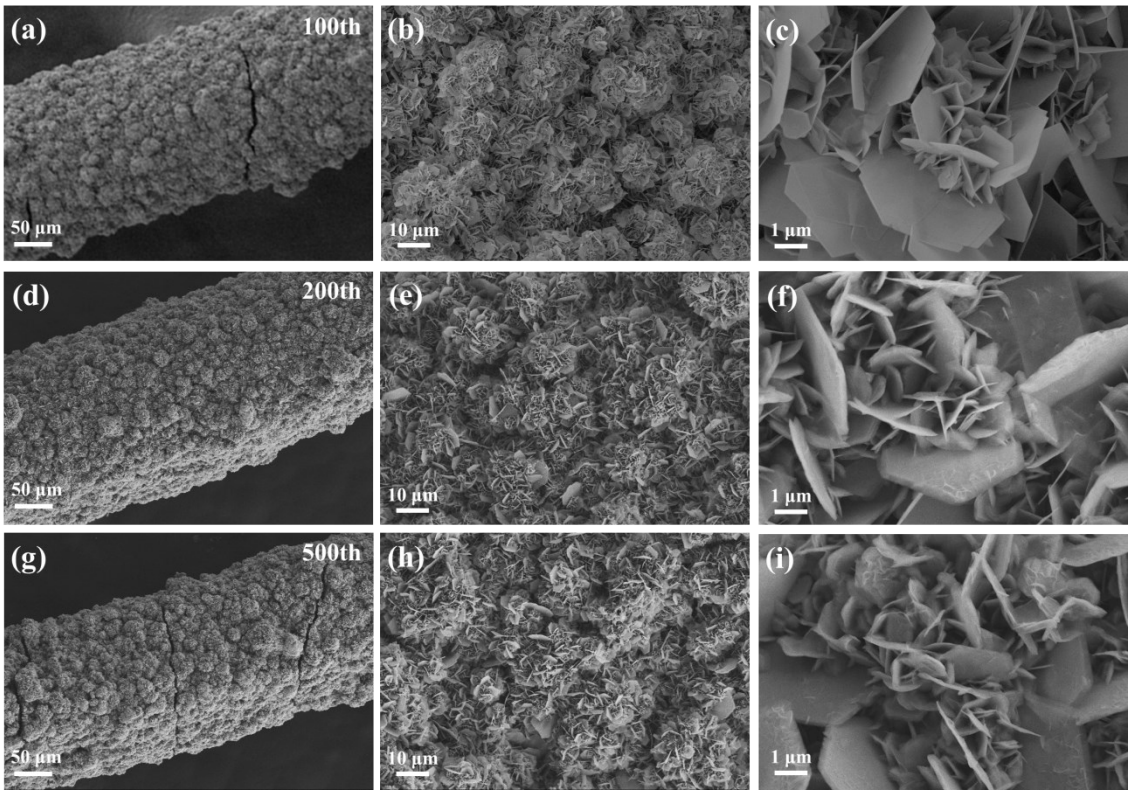

Fig. S11. SEM images of the Zn NSs@CNT fibers after (a-c) 100, (d-f) 200 and (g-i) 500 cycles test. (Noted: The cycling test for our FZHSC was performed at a current density of 7.12 mA cm^{-2} in a 3 M $Zn(CF_3SO_3)_2$ aqueous electrolyte instead of polymer gel electrolyte. Because the morphology of the Zn NSs@CNT fiber was covered by polymer gel in Fig. 5e, it cannot be observed.)

References

1. M. Miao, J. McDonnell, L. Vuckovic and S. C. Hawkins, *Carbon*, 2010, **48**, 2802-2811.
2. Y. Bu, T. Sun, Y. Cai, L. Du, O. Zhuo, L. Yang, Q. Wu, X. Wang and Z. Hu, *Adv. Mater.*, 2017, **29**, 1700470.
3. J. Pokrzywinski, J. K. Keum, R. E. Ruther, E. C. Self, M. Chi, H. Meyer Iii, K. C. Littrell, D. Aulakh, S. Marble, J. Ding, M. Wriedt, J. Nanda and D. Mitlin, *J. Mater. Chem. A*, 2017, **5**, 13511-13525.
4. Y. Zhang, S. Liu, X. Zheng, X. Wang, Y. Xu, H. Tang, F. Kang, Q.-H. Yang and J. Luo, *Adv. Funct. Mater.*, 2017, **27**, 1604687.
5. K. Jayaramulu, D. P. Dubal, B. Nagar, V. Ranc, O. Tomanec, M. Petr, K. K. R. Datta, R. Zboril, P. Gómez-Romero and R. A. Fischer, *Adv. Mater.*, 2018, **30**, 1705789.
6. Q. Zhang, K. Han, S. Li, M. Li, J. Li and K. Ren, *Nanoscale*, 2018, **10**, 2427-2437.
7. X. Yu, J. Lu, C. Zhan, R. Lv, Q. Liang, Z.-H. Huang, W. Shen and F. Kang, *Electrochim. Acta*, 2015, **182**, 908-916.
8. F. Zhang, T. Liu, M. Li, M. Yu, Y. Luo, Y. Tong and Y. Li, *Nano Lett.*, 2017, **17**, 3097-3104.
9. J. Pang, W. Zhang, J. Zhang, G. Cao, M. Han and Y. Yang, *Green Chem.*, 2017, **19**, 3916-3926.
10. P. Yu, Y. Liang, H. Dong, H. Hu, S. Liu, L. Peng, M. Zheng, Y. Xiao and Y. Liu, *ACS Sustain. Chem. Eng.*, 2018, **6**, 15325-15332.
11. H. Wang, M. Wang and Y. Tang, *Energy Storage Mater.*, 2018, **13**, 1-7.
12. P. Zhang, Y. Li, G. Wang, F. Wang, S. Yang, F. Zhu, X. Zhuang, O. G. Schmidt and X. Feng, *Adv. Mater.*, 2019, **31**, e1806005.
13. X. Zhang, Z. Pei, C. Wang, Z. Yuan, L. Wei, Y. Pan, A. Mahmood, Q. Shao and Y. Chen, *Small*, 2019, **15**, e1903817.
14. Z. Jian, N. Yang, M. Vogel, S. Leith, A. Schulte, H. Schönherr, T. Jiao, W. Zhang, J. Müller, B. Butz and X. Jiang, *Adv. Energy Mater.*, 2020, **18**, 2002202.
15. Y. Shao, Z. Sun, Z. Tian, S. Li, G. Wu, M. Wang, X. Tong, F. Shen, Z. Xia, V. Tung, J. Sun and Y. Shao, *Adv. Funct. Mater.*, 2020, **31**, 2007843.
16. J. Zeng, L. Dong, L. Sun, W. Wang, Y. Zhou, L. Wei and X. Guo, *Nano-Micro Lett.*, 2020, **13**, 19.
17. H. Zhang, Q. Liu, Y. Fang, C. Teng, X. Liu, P. Fang, Y. Tong and X. Lu, *Adv. Mater.*, 2019, **31**, e1904948.
18. S. Chen, L. Ma, K. Zhang, M. Kamruzzaman, C. Zhi and J. A. Zapien, *J. Mater. Chem. A*, 2019, **7**, 7784-7790.
19. Y. Lu, Z. Li, Z. Bai, H. Mi, C. Ji, H. Pang, C. Yu and J. Qiu, *Nano Energy*, 2019, **66**, 104132.
20. Y. Meng, Y. Zhao, C. Hu, H. Cheng, Y. Hu, Z. Zhang, G. Shi and L. Qu, *Adv. Mater.*, 2013, **25**, 2326-2331.
21. Y. Fu, X. Cai, H. Wu, Z. Lv, S. Hou, M. Peng, X. Yu and D. Zou, *Adv. Mater.*, 2012, **24**, 5713-5718.
22. J. Ren, W. Bai, G. Guan, Y. Zhang and H. Peng, *Adv. Mater.*, 2013, **25**, 5965-5970.
23. D. Yuan, B. Li, J. Cheng, Q. Guan, Z. Wang, W. Ni, C. Li, H. Liu and B. Wang, *J. Mater. Chem. A*, 2016, **4**, 11616-11624.
24. Z. Yu, B. Duong, D. Abbitt and J. Thomas, *Adv. Mater.*, 2013, **25**, 3302-3306.
25. Y. Zeng, Y. Meng, Z. Lai, X. Zhang, M. Yu, P. Fang, M. Wu, Y. Tong and X. Lu, *Adv. Mater.*, 2017, **29**, 1702698
26. L. Liu, Y. Yu, C. Yan, K. Li and Z. Zheng, *Nat. Commun.*, 2015, **6**, 7260.